Combining statistical shape model and principal component analysis to estimate left ventricular volume and ejection fraction

Liu, Dawei, Dangi, Shusil, Schwarz, Karl, Linte, Cristian

Dawei Liu, Shusil Dangi, Karl Q. Schwarz, Cristian A. Linte, "Combining statistical shape model and principal component analysis to estimate left ventricular volume and ejection fraction," Proc. SPIE 11319, Medical Imaging 2020: Ultrasonic Imaging and Tomography, 113190E (16 March 2020); doi: 10.1117/12.2550650

SPIE.

Event: SPIE Medical Imaging, 2020, Houston, Texas, United States

Combining Statistical Shape Model and Principal Component Analysis to Estimate Left Ventricular Volume and Ejection Fraction

Dawei Liu[a], Shusil Dangi[a], Karl Q. Schwarz[b,c], and Cristian A. Linte[a,d]

[a]Center for Imaging Science, Rochester Institute of Technology, Rochester, NY, USA
[b]Medicine, Cardiology, University of Rochester Medical Center, Rochester, NY, USA
[c]Anesthesiology and Perioperative Medicine, University of Rochester Medical Center, Rochester, NY, USA
[d]Biomedical Engineering, Rochester Institute of Technology, Rochester, NY, USA

ABSTRACT

Left ventricular ejection fraction (LVEF) assessment is instrumental for cardiac health diagnosis, patient management, and patient eligibility for participation in clinical studies. Due to its non-invasiveness and low operational cost, ultrasound (US) imaging is the most commonly used imaging modality to image the heart and assess LVEF. Even though 3D US imaging technology is becoming more available, cardiologists dominantly use 2D US imaging to visualize the LV blood pool and interpret its area changes between end-systole and end-diastole. Our previous work showed that LVEF estimates based on area changes are significantly lower than the true volume-based estimates by as much as 13%,[1] which could lead to unnecessary and costly therapeutic decisions. Acquiring volumetric information about the LV blood pool necessitates either time-consuming 3D reconstruction or 3D US image acquisition. Here, we propose a method that leverages on a statistical shape model (SSM) constructed from 13 landmarks depicting the LV endocardial border to estimate a new patient's LV volume and LVEF. Two methods to estimate the 3D LV geometry with and without size normalization were employed. The SSM was built using the 13 landmarks from 50 training patient image datasets. Subsequently, the Mahalanobis distance (with size normalization) or the vector distance (without size normalization) between an incoming patient's LV landmarks and each shape in the SSM were used to determine the weights each training patient contributed to describing the new, incoming patient's LV geometry and associated blood pool volume. We tested the proposed method to estimate the LV volumes and LVEF for 16 new test patients. The estimated LVEFs based on Mahalanobis distance and vector distance were within 2.9% and 1.1%, respectively, of the ground truth LVEFs calculated from the 3D reconstructed LV volumes. Furthermore, the viability of using fewer principal components (PCs) to estimate the LV volume was explored by reducing the number of PCs retained when projecting landmarks onto PCA space. LVEF estimated based on 3 PCs, 5 PCs, and 10 PCs are within 6.6%, 5.4%, and 3.3%, respectively, of LVEF estimates using the full set of 39 PCs.

Keywords: ultrasound image analysis; statistical shape model; principal component analysis; 3D reconstruction

1. INTRODUCTION

As a critical indicator of the cardiac function, the left ventricular ejection fraction (LVEF) measures the ventricular contraction efficiency in the form of the ratio between the LV stroke volume and diastolic volume. LVEF is used in vast aspects of clinical applications such as a patient management metric and clinical study eligibility criterion. In our previous work,[1] we discussed the realities in clinical practice and challenges for cardiologists to assess LVEF based on true LV volumes instead of visually estimating LVEF based on 2D images. Notwithstanding these obstacles, it is paramount that we persistently pursue a method that allows clinicians to calculate LVEF based on volumetric data. Calculating LVEF accurately will reduce the occurrences of unnecessary therapeutic treatments that are costly[2] and detrimental to a patient's quality of life. To enable clinicians to calculate LVEF

Medical Imaging 2020: Ultrasonic Imaging and Tomography, edited by Brett C. Byram, Nicole V. Ruiter,
Proc. of SPIE Vol. 11319, 113190E · © 2020 SPIE · CCC code: 1605-7422/20/$21 · doi: 10.1117/12.2550650

based on volumes practically, a method that demands minimal manual input and delivers results quickly must be devised.

A statistical shape model (SSM) approach was employed in numerous studies for different applications in the field cardiology. A group of LV geometries is used to assemble an SSM that encompasses all of the spatial coordinates of the LV surfaces. The mean shape is calculated from the group and then used to determine an individual's deviation from the mean. Some categorical conclusion is drawn based on the individual's deviation from the mean shape. Commonly, SSMs were used to represent characteristics of innumerable shapes of the LV for a population of human subjects with reasonable accuracies.[3] The generalized characteristics were used to study LV morphology caused by various cardiac health conditions.[4,5] Others incorporate principal component analysis (PCA) into the SSM to analyze the modes of variation in the geometric characteristics.[6–10]

We propose a SSM approach with and without size normalization to estimate a new LV systolic and diastolic volume and subsequently calculate the LVEF based on only 13 landmarks that define the LV endocardial borders. The 13 landmarks are empirically known characteristic features of an LV consisting of the LV apex (1), mitral valve hinges (6), and the midpoints of the endocardial contours (6). The SSM is constructed from a population of 50 patient-specific US tri-plane images. PCA was performed to eventually allow LV volume and LVEF estimations for the test patients using fewer PCs than the full 39 PCs.

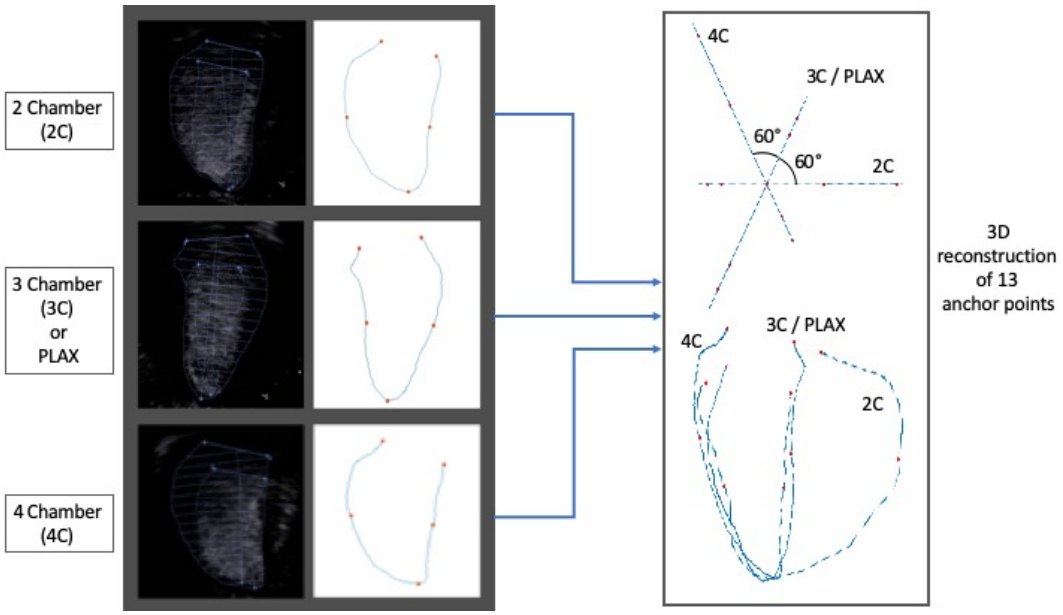

Figure 1. In each tomographic view of the LV, 5 landmarks (red points) are located on the endocardial border (blue contours). From the 3 tomographic views that are roughly 60 degrees apart, 13 unique landmarks are reconstructed from 2D to 3D.

2. METHODS

For this study, we had available 66 patient-specific tri-plane US image datasets, of which 50 were used as training data for constructing the SSM and 16 were used as testing data for LV volume and LVEF estimations. For each image dataset, three tomographic views were captured at roughly 60 degrees apart: 2-chamber (2C) view, 3-chamber view (3C), and 4-chamber (4C) view. Sometimes, parasternal long-axis (PLAX) view was used due to image capture difficulty. Ground truth LV blood pools were segmented and their 3D reconstructed volumes were obtained previously. The coordinates of the landmarks were first defined from 2D US images, then transformed, as shown in Figure 1, into 3D coordinates using the reconstruction algorithm employed in our earlier work.[11] After 3D reconstruction of the landmarks, their coordinates are structured as detailed in Equation 1. For each landmark, there are X, Y, and Z coordinates. The subscripts describe which landmark each coordinate correspond

to. "Left hinge" refers to the mitral valve hinge on the left side of the endocardial contour, "left midpoint" refers to the midpoint of the left half of the endocardial contour, and "apex" refers to the generally stationary apex of the left ventricle. Both the "right hinge" and "right midpoint" refer to the landmarks on the right side of the endocardial contour. "2C", "3C/PLAX", and "4C" refer to which tomographic view the coordinate represents. Since there is only one unique apex for the left ventricle, only one set of coordinates is used to represent the apex location.

$$Anchors_{3D} = \begin{bmatrix} X_{left\ hinge-2C} & Y_{left\ hinge-2C} & Z_{left\ hinge-2C} \\ X_{left\ midpoint-2C} & Y_{left\ midpoint-2C} & Z_{left\ midpoint-2C} \\ X_{apex} & Y_{apex} & Z_{apex} \\ X_{right\ midpoint-2C} & Y_{right\ midpoint-2C} & Z_{right\ midpoint-2C} \\ X_{right\ hinge-2C} & Y_{right\ hinge-2C} & Z_{right\ hinge-2C} \\ X_{left\ hinge-3C/PLAX} & Y_{left\ hinge-3C/PLAX} & Z_{left\ hinge-3C/PLAX} \\ X_{left\ midpoint-3C/PLAX} & Y_{left\ midpoint-3C/PLAX} & Z_{left\ midpoint-3C/PLAX} \\ X_{right\ midpoint-3C/PLAX} & Y_{right\ midpoint-3C/PLAX} & Z_{right\ midpoint-3C/PLAX} \\ X_{right\ hinge-3C/PLAX} & Y_{right\ hinge-3C/PLAX} & Z_{right\ hinge-3C/PLAX} \\ X_{left\ hinge-4C} & Y_{left\ hinge-4C} & Z_{left\ hinge-4C} \\ X_{left\ midpoint-4C} & Y_{left\ midpoint-4C} & Z_{left\ midpoint-4C} \\ X_{right\ midpoint-4C} & Y_{right\ midpoint-4C} & Z_{right\ midpoint-4C} \\ X_{right\ hinge-4C} & Y_{right\ hinge-4C} & Z_{right\ hinge-4C} \end{bmatrix} = [13 \times 3] \quad (1)$$

The 3D coordinates of the 13 landmarks for the 50 training datasets were assembled into the SSM of dimension 50 x 13 x 3. Encompassing the landmark coordinates from all 50 training datasets is a prerequisite for constructing the SSM. LV shapes vary in size, so the alignment scheme was carefully determined. Since we will examine the LV volume estimation performances with and without size normalization, it was decided not to scale the training LV shapes based on their sizes while aligning them. The axis along which the three tomographic views intersect for each training patient was used as the alignment axis when combining the 50 datasets into the SSM. Once the landmarks of the 50 training datasets were aligned along the axis, their centers of mass along the alignment axis were calculated and offset to zero. Finally, the centers of mass of all 50 LV shapes locate at the origin, hence, (0, 0, 0) in 3D. The SSM is now ready to be used for LV volume estimations.

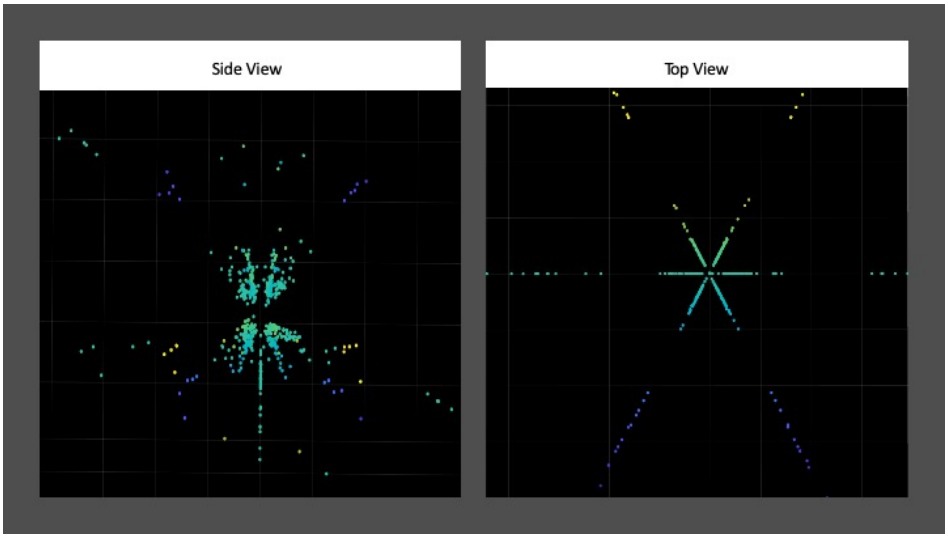

Figure 2. Point cloud representation of the 13 landmarks of all 50 training datasets.

We estimated the systolic and diastolic LV volumes and computed the associated LVEFs for the 16 test patients based on either the Mahalanobis distances or vector distance in PCA space between a test patient and

each of the training patient (with index i) in the SSM. The Mahalanobis distance calculation normalizes the sizes of LV shapes by the inverse covariance matrix of the SSM. On the other hand, the PCA vector distance calculation takes the LV sizes into account. These two approaches help determine the effect of size in SSM-based LV volume estimations.

The Mahalanobis distance[12] M_i is based on the Euclidean distance $(test - train_i)$, its transpose, and normalized by the inverse covariance matrix C^{-1} of the SSM. This operation removes the size differences in the data. The calculation of Mahalanobis distance is carried out using Equation 2 below:

$$M_i = \sqrt{(test - train_i)^T \; C^{-1} \; (test - train_i)} \tag{2}$$

In contrast to the Mahalanobis distance calculation based in Euclidean space, the PCA vector distance that takes the LV size into consideration is based in PC space. Before calculating the vector distance in PC space, the SSM dimension was transformed from 50 x 13 x 3 to 50 x 39. The Gramian matrix of the SSM with the dimension of 39 x 39 was obtained (Equation 3) so that the eigenvalues and eigenvectors of the SSM could be calculated by eigen-decomposition.

$$A' = [50 \times 39]^T \; [50 \times 39] = [39 \times 50] \; [50 \times 39] = [39 \times 39] \tag{3}$$

Using the eigen-decomposition, the eigenvalues and eigenvectors of the SSM were calculated as shown in Equation 4, where $\underline{\lambda}$ is the diagonal matrix consisting of eigenvalues and $\underline{D}$ is the matrix of corresponding eigenvectors.

$$\underline{A}^{'} \; \underline{D} = \underline{\lambda} \; \underline{D} \tag{4}$$

The eigenvectors were sorted with respect to their corresponding eigenvalues in descending order, which allowed for PC dimensionality reduction in the later analysis. All landmarks of the 66 patient datasets were projected onto the PC space by multiplying with the eigenvector matrix so that they are represented as a linear combination of the 39 modes of variation in the SSM. The vector distances in PC space V_i between a test patient and each training patient in PC space were calculated. The Mahalanobis and PCA vector distances were used to determine the weight w_i each training patient's LV volume V_i contributed to a new test patient's LV volume estimate, as shown by Equations 5 and 6.

$$w_i = \frac{\sum_{i=0}^{50} M_i}{M_i} \; or \; \frac{\sum_{i=0}^{50} V_i}{V_i} \tag{5}$$

$$V_{estimated} = \sum_{i=0}^{50} w_i V_i \tag{6}$$

The reference volume V_i of each patient patient is calculated from LV volumes reconstructed using the algorithm explained in our previous work.[1]

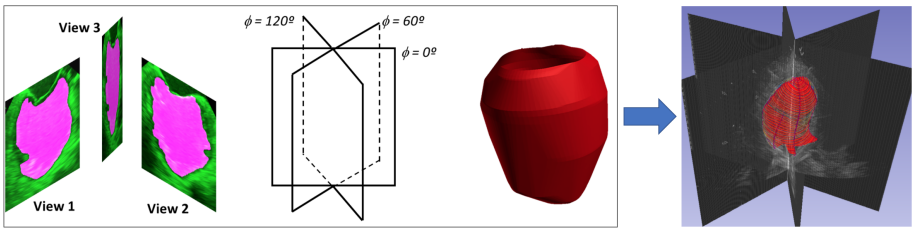

Figure 3. An illustration of the 3D reconstruction workflow.

3. RESULTS

Using the SSM generated from 50 training patient datasets, the LV systolic and diastolic volumes of the 16 test patient datasets were estimated based on Mahalanobis distance (Estimate 1) and vector distance in PCA space (Estimate 2). The stroke volumes were calculated as the difference between diastolic and systolic volumes, and the LVEFs were computed by dividing the stroke volume by the corresponding diastolic volume. Comparing the estimates to the values from 3D reconstruction, LVEFs based on Mahalanobis distance and vector distance are within 2.9% and 1.1%, respectively, of the ground truth volumes. Noticeably, the estimates based on Mahalanobis distance are generally further from the ground truth than those based on vector distance in PCA space, which implies that the size effect of LV shapes makes a meaningful contribution to estimation accuracy.

Table 1. Summary of the estimated volumes and LVEFs using the SSM approach based on Mahalanobis distance and vector distance in PCA space and the ground truths values from 3D LV volume reconstruction.

Method	Mean±Standard Error*		
	LVEF [%]	Stroke Volume [ml]	Diastolic Volume [ml]
Image Data	55.6 ± 4.6	59.6 ± 3.94	125.8 ± 17.3
Estimate 1	$58.5.1 \pm 5.1$	64.4 ± 3.9	130.1 ± 17.4
Estimate 2	54.5 ± 4.6	57.3 ± 4.2	123.3 ± 17.3

* *Standard Error = Standard Deviation* / $\sqrt{Number\ of\ Samples}$

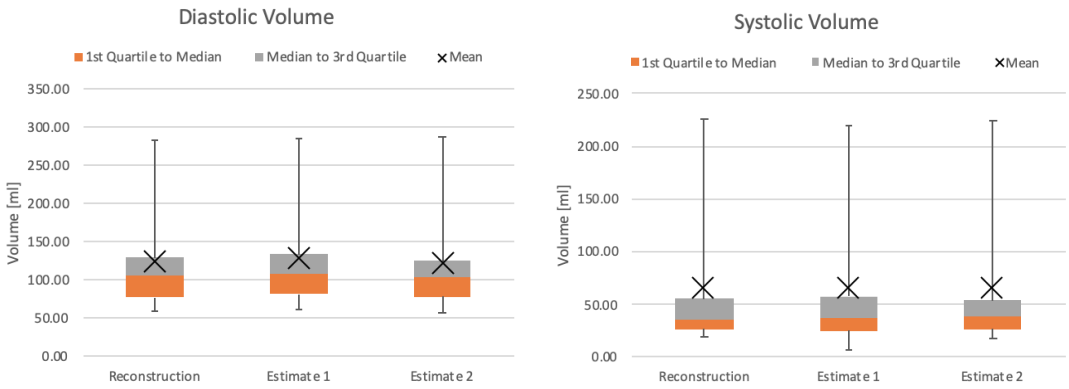

Figure 4. Reference and estimated volumes using Mahalanobis distance (Estimate 1) and vector distance (Estimate 2).

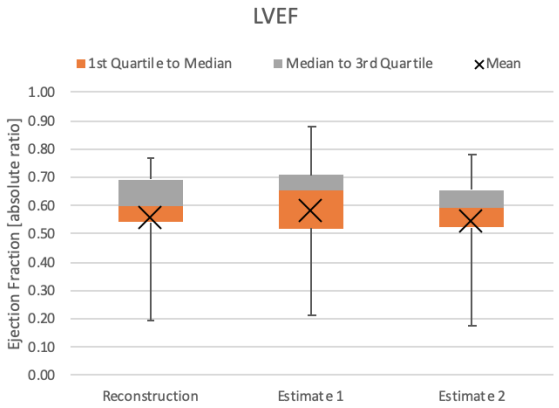

Figure 5. Reference and estimated LVEFs using Mahalanobis distance (Estimate 1) and vector distance (Estimate 2).

Additionally, we extended the PC analysis by varying the number of the PCs retained to estimate the LV volumes. Instead of using all 39 PCs to estimate the LV volumes, only the most dominant 3, 5, and 10 PCs, based on the same number of highest corresponding eigenvalues, were used instead. Similarly, the stroke volumes and LVEFs were calculated from the estimated systolic and diastolic volumes using these fewer PCs. The LVEF estimated using only 3, 5, and 10 PCs, was on average 6.6%, 5.4%, and 3.3%, respectively, higher than the LVEF computed using all 39 PCs. More importantly, the ANOVA statistical analysis gave a p-value of 0.78, an F value of 0.36, and a critical F value of 2.76. Since the p-value is higher than 0.05 and the F value is lower than the critical F value, the ANOVA results confirmed that estimating using only 3, 5, and 10 PCs were not significantly different from using all 39 PCs.

Table 2. Summary of the LVEFs calculated from systolic and diastolic volumes estimated vector distance in PCA space using all 39 PCs compared to only using 3, 5, and 10 PCs.

Number of PCs	3	5	10	39
Systolic Volume Mean ± Standard Error [%]	56.82 ± 17.3	57.94 ± 15.7	62.73 ± 17.8	66.04 ± 17.1
Diastolic Volume Mean ± Standard Error [%]	118.1 ± 17.4	119.7 ± 17.2	122.3 ± 17.3	123.3 ± 17.3
Stroke Volume Mean ± Standard Error [%]	61.2 ± 4.4	61.7 ± 4.4	59.6 ± 4.5	57.3 ± 4.2
LVEF Mean ± Standard Error [%]	61.1 ± 5.0	59.9 ± 4.7	57.8 ± 5.0	54.5 ± 4.6
LVEF Percent Error* [%]	9.9	7.7	4.0	2.0

* $Percent\ Error = |Estimated\ LVEF - Image\ data\ LVEF|\ /\ Image\ data\ LVEF * 100\%$

All 39 eigenvalues were normalized so that they sum to unity. Consequently, each normalized eigenvalue denotes how much its corresponding eigenvector represents the SSM. Since the eigenvalues were sorted in descending order, accumulations of 1 to 39 eigenvalues were calculated to aid the understanding of how many PCs are necessary to reasonably represent the SSM to estimate an LV volume. As illustrated in Figure 6, the margin of return dramatically decreases when over 12 eigenvalues were accumulated. Hence, the estimation accuracy improves much more slowly when more than 12 PCs are used.

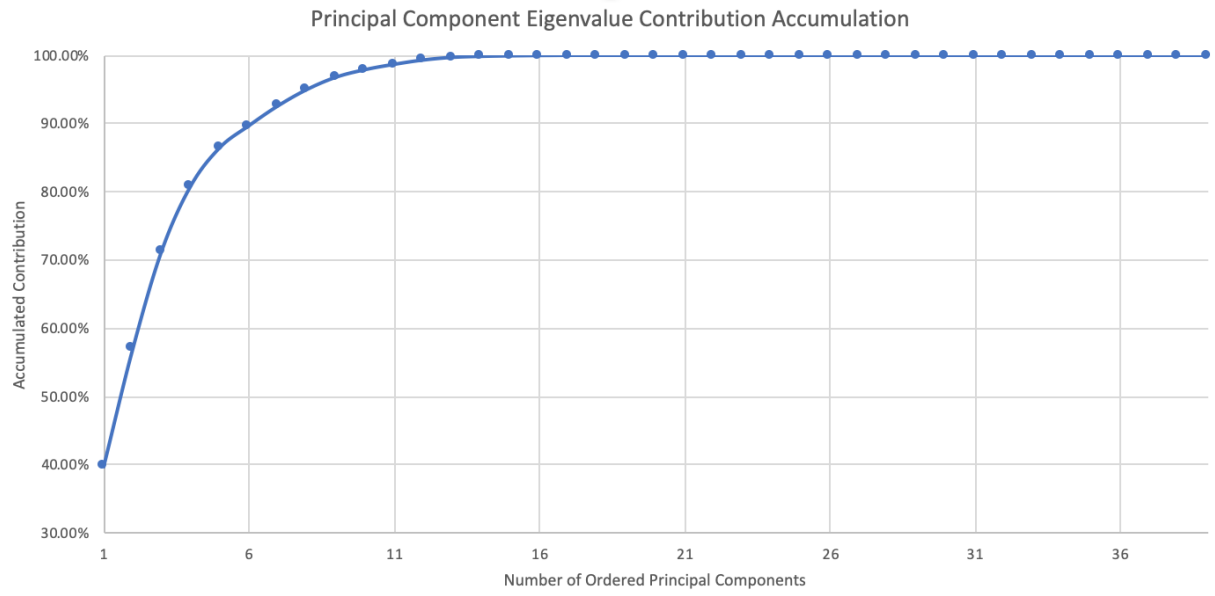

Figure 6. By accumulating the sorted eigenvalues associated with the eigenvectors, the plot illustrates the percentage of contribution each PC makes towards describing an LV shape.

4. DISCUSSION, CONCLUSION, AND FUTURE WORK

Our SSM approach for estimating LV volume and LVEF based on Mahalanobis distance and vector distance in PCA space delivered promising prospect to obtaining reasonably more accurate volume-based LVEF estimates than area-based estimates currently in practice. Specifically, the estimation method based on PCA vector distance achieved results closer to the ground truths than the Mahalanobis distance method. The PCA-based method also allows the usage of only a few modes of variation, and yet maintains an acceptable accuracy in the LVEF estimation. As pointed out by other researchers,[7,13] the first three to five PCs describe the majority of the shape variances in SSM. In our case, the first three and five PCs describe 71.4% and 86.5%, respectively, of the overall variances in our SSM. In the future, we plan to obtain true 3D US imaging data from our collaborating clinicians, such that the performance of our model can be further improved and evaluated.

ACKNOWLEDGMENTS

Research reported in this publication was supported by the National Institute of General Medical Sciences of the National Institutes of Health under Award No. R35GM128877 and by the Office of Advanced Cyberinfrastructure of the National Science Foundation under Award No. 1808530.

REFERENCES

[1] Liu, D., Peck, I., Dangi, S., Schwarz, K., and Linte, C., "Left ventricular ejection fraction assessment: unraveling the bias between area- and volume-based estimates," in [*Proc. SPIE Medical Imaging - Ultrasonic Imaging and Tomography*], **10955**, 109550T–1–8 (2019).

[2] Groeneveld, P. W., Matta, M. A., Suh, J. J., Heidenreich, P. A., and Shea, J. A., "Costs and quality-of-life effects of implantable cardioverter-defibrillators," *The American Journal of Cardiology* **98**(10), 1409 – 1415 (2006).

[3] Suinesiaputra, A., Ablin, P., Alb, X., Alessandrini, M., Allen, J., Bai, W., Cimen, S., Claes, P., Cowan, B., D'hooge, J., Duchateau, N., Ehrhardt, J., Frangi, A., Gooya, A., Grau, V., Lekadir, K., Lu, A., Mukhopadhyay, A., Oksuz, I., and Medrano-Gracia, P., "Statistical shape modeling of the left ventricle: Myocardial infarct classification challenge," *IEEE Journal of Biomedical and Health Informatics* **22**, 503–15 (2017).

[4] Bruse, J. L., Ntsinjana, H., Capelli, C., Biglino, G., McLeod, K., Sermesant, M., Pennec, X., Hsia, T.-Y., Schievano, S., and Taylor, A., "Cmr-based 3d statistical shape modelling reveals left ventricular morphological differences between healthy controls and arterial switch operation survivors," *Journal of Cardiovascular Magnetic Resonance* **18** (2016).

[5] Farrar, G., Suinesiaputra, A., Gilbert, K., Perry, J. C., Hegde, S., Marsden, A., Young, A. A., Omens, J. H., and McCulloch, A. D., "Atlas-based ventricular shape analysis for understanding congenital heart disease," *Progress in Pediatric Cardiology* **43**, 61 – 9 (2016).

[6] Medrano-Gracia, P., Cowan, B. R., Ambale-Venkatesh, B., Bluemke, D. A., Eng, J., Finn, J. P., Fonseca, C. G., Lima, J. A., Suinesiaputra, A., and Young, A. A., "Left ventricular shape variation in asymptomatic populations: the multi-ethnic study of atherosclerosis," *Journal of Cardiovascular Magnetic Resonance* **16**, 56 (2014).

[7] Piras, P., Teresi, L., Puddu, P., Concetta, T., Young, A., Suinesiaputra, A., and Medrano-Gracia, P., "Morphologically normalized left ventricular motion indicators from mri feature tracking characterize myocardial infarction," *Scientific Reports* **7** (2017).

[8] Remme, E. W., Young, A. A., Augenstein, K. F., Cowan, B., and Hunter, P. J., "Extraction and quantification of left ventricular deformation modes," *IEEE Transactions on Biomedical Engineering* **51**, 1923–31 (2004).

[9] Tejman-Yarden, S., Bratincsak, A., Bachner-Hinenzon, N., Khamis, H., Rzasa, C., Adam, D., Printz, B. F., and Perry, J. C., "Left ventricular mechanical property changes during acute av synchronous right ventricular pacing in children," *Pediatric Cardiology* **37**, 106–111 (2016).

[10] Zhang, X., Cowan, B. R., Bluemke, D. A., Finn, J. P., Fonseca, C. G., Kadish, A. H., Lee, D. C., Lima, J. A. C., Suinesiaputra, A., Young, A. A., and Medrano-Gracia, P., "Atlas-based quantification of cardiac remodeling due to myocardial infarction," *PLOS ONE* , 1–13 (2014).

[11] Dangi, S., Ben-Zikri, Y. K., Cahill, N., Schwarz, K. Q., and Linte, C. A., "Endocardial left ventricle feature tracking and reconstruction from tri-plane trans-esophageal echocardiography data," in [*Medical Imaging 2015: Image-Guided Procedures, Robotic Interventions, and Modeling*], **9415**, 941505 (Mar. 2015).

[12] Mclachlan, G., "Mahalanobis distance," *Resonance* **4**, 20–26 (06 1999).

[13] Medrano-Gracia, P., Cowan, B. R., Finn, J. P., Fonseca, C. G., Kadish, A. H., Lee, D. C., Tao, W., and Young, A. A., "The cardiac atlas project: Preliminary description of heart shape in patients with myocardial infarction," in [*Statistical Atlases and Computational Models of the Heart*], Camara, O., Pop, M., Rhode, K., Sermesant, M., Smith, N., and Young, A., eds., 46–53 (2010).